

Boltzmann H function and entropy in the plasma sheet

Richard L. Kaufmann¹ and William R. Paterson²

Received 29 December 2008; revised 18 February 2009; accepted 23 February 2009; published 8 May 2009.

[1] Boltzmann's H function was evaluated using 10 years of 1-min distribution functions. These results were used to study the long-term averaged spatial distributions of four entropy parameters. The average entropy density $s_a(\mathbf{x})$, where $a = i$ for ions and $a = e$ for electrons, increased when moving Earthward or toward the flanks. The magnitudes of these entropy changes were similar for ions and electrons. The entropy per unit flux tube $S_{f,a}(\mathbf{x})$ decreased when moving Earthward or toward midnight. The spatial changes of $s_a(\mathbf{x})$ and of $S_{f,a}(\mathbf{x})$ were attributed primarily to variations of the particle density $n_a(\mathbf{x})$ and of the particle content of each unit flux tube $N_f(\mathbf{x})$, respectively. A dimensionless parameter $(S/Nc_v)_{H,i}$ that is proportional to the average entropy per ion increased when moving Earthward or toward midnight near the neutral sheet. The dimensionless parameter proportional to the entropy per ion that would exist in a plasma with the measured pressure and density but with a Maxwellian distribution function $(S/Nc_v)_{P,i}$ was also calculated. Differences between $(S/Nc_v)_{P,i}$ and $(S/Nc_v)_{H,i}$ showed that the plasma was closer to equilibrium near the neutral sheet at $x = -10 R_E$ than at $x = -28 R_E$. These gradients of the entropy per ion and of the deviations from equilibrium suggest that nonadiabatic processes and particle scattering are significant throughout the region studied.

Citation: Kaufmann, R. L., and W. R. Paterson (2009), Boltzmann H function and entropy in the plasma sheet, *J. Geophys. Res.*, *114*, A00D04, doi:10.1029/2008JA014030.

1. Introduction

[2] Entropy has been studied in the plasma sheet primarily as a way to identify regions where or time periods when the plasma was heated or cooled. It is the change in entropy $dS \geq dQ/T$ that is of interest in such studies, where dS is the entropy change of a fixed group of N particles, dQ is the heat absorbed by these particles at temperature T , and the equal sign holds if the process is reversible. The present project was intended to see if a study of the Boltzmann H function could explain currently unresolved features of the entropy distribution in the plasma sheet. This introduction defines the parameters that were examined and describes some of the problems that arise in the interpretation of entropy measurements.

1.1. Basic Fluid Parameters

[3] Ions and electrons were treated as separate fully ionized nonrelativistic ideal monatomic gases. Since ion mass information was not available, we assumed that all the ions were protons. Several fluid parameters [Rossi and Olbert, 1970] were used to study the long-term averaged

spatial variations of entropy in the plasma sheet. The ion and electron number densities are defined as

$$n_a(\mathbf{x}, t) = \int f_a(\mathbf{x}, \mathbf{v}, t) d^3v, \quad (1)$$

where $a = i$ or e for the ion or the electron fluid and $f_a(\mathbf{x}, \mathbf{v}, t)$ is the measured single-particle velocity distribution function. The bulk velocity vectors

$$\mathbf{V}_a(\mathbf{x}, t) = \int \mathbf{v} f_a(\mathbf{x}, \mathbf{v}, t) d^3v / n_a(\mathbf{x}, t) \quad (2)$$

are needed to evaluate the individual pressure tensors

$$\mathbf{P}_a(\mathbf{x}, t) = \int m_a [\mathbf{v} - \mathbf{V}_a(\mathbf{x}, t)] [\mathbf{v} - \mathbf{V}_a(\mathbf{x}, t)] f_a(\mathbf{x}, \mathbf{v}, t) d^3v, \quad (3)$$

where m_a is the particle mass.

[4] The thermal energy of a species, or the kinetic energy density in the frame moving with the bulk velocity of that species is $1/2 \text{Tr}[\mathbf{P}_a]$. Temperature tensors $\mathbf{T}_a(\mathbf{x}, t)$ are defined by

$$\mathbf{P}_a(\mathbf{x}, t) = n_a(\mathbf{x}, t) k \mathbf{T}_a(\mathbf{x}, t), \quad (4)$$

where k is Boltzmann's constant. The scalar kinetic temperature is $T_a = 1/3 \text{Tr}[\mathbf{T}_a]$.

¹Department of Physics, University of New Hampshire, Durham, New Hampshire, USA.

²Department of Atmospheric and Planetary Sciences, Hampton University, Hampton, Virginia, USA.

1.2. Entropy Parameters Used in Previous Studies

[5] One commonly used entropy parameter is P_a/n_a^γ , where $P_a = 1/3 \text{Tr}[P_a]$ and a specific heat ratio of $\gamma = 5/3$ is used for an ideal monatomic gas. The P_a/n_a^γ parameter is a measure of the entropy per particle, and was used by *Goertz and Baumjohann* [1991] and by *Huang et al.* [1992] to study the plasma sheet. These papers concluded that motion through the interface between the plasma sheet boundary layer (PSBL) and the central plasma sheet (CPS) was nearly adiabatic, but that nonadiabatic processes appeared to take place during substorms.

[6] Other frequently used parameters are $P_a V_f^{5/3}$ and $T_a V_f^{2/3} = P_a V_f^{5/3} / (N_f k)$. The energy parameter $\lambda_a = 3/2 k T_a V_f^{2/3}$ is constant during the adiabatic compression of a fixed number of particles if $f_a(\mathbf{x}, \mathbf{v}, t)$ remains isotropic [Wolf, 1983]. The volume V_f and the number of ions and of electrons N_f refer to a tube, integrated from the neutral sheet to the ionosphere, containing 1 Wb of magnetic flux. Although $P_a/n_a^{5/3}$ depends only upon locally measured fluid parameters, a magnetic field model is needed to determine $P_a V_f^{5/3}$, $T_a V_f^{2/3}$, and λ_a . *Erickson and Wolf* [1980] compared long-term averages of $P_a V_f^{5/3}$ to a series of magnetic field models to show that, near midnight, the average entropy per unit flux tube depends strongly upon the GSM x location of its equatorial crossing point.

[7] Problems arise when evaluating some entropy parameters. The ion and electron bulk velocities $\mathbf{V}_a(\mathbf{x}, t)$ must be calculated for every data point before it's possible to determine the ion and electron pressures (equation (3)) or temperatures (equation (4)). However, bulk velocities fluctuate rapidly, and the evaluation of \mathbf{V}_e is especially difficult. It's also hard to interpret average spatial variations of some entropy parameters. For example, plasma waves that are generated or absorbed within a flux tube will cool or heat the plasma. These waves cannot be studied directly in our analysis, but their effects influence the properties of the 10-year averaged models.

[8] The predominantly cross-tail gradient and curvature drifts are energy and charge dependent. It therefore is not possible to define a flux tube convection velocity such that all ions or all electrons remain within a unit flux tube. For example, the gradient of the ion density is studied by splitting the ions into many groups, following each group of ions by assuming some parameter is conserved, and then summing the partial densities of the ions that arrive at a desired point [Spence and Kivelson, 1993; Garner et al., 2003; Wang et al., 2006]. The groups of ions contributing to the density at a desired point therefore come from various initial locations that are characterized by different source distribution functions.

[9] Reconnection is a process that makes interpretation of long-term averaged spatial gradients particularly difficult. The spatial gradients of $P_a V_f^{5/3}$ and $T_a V_f^{2/3}$ would be the same if N_f was uniform. However, reconnection changes the volume, the shape, the number of particles, and the entropy within a unit flux tube. Gradients of the time averaged $N_f(\mathbf{x})$ present the biggest problem. For time averaged unit flux tube variables, \mathbf{x} refers to the point along a flux tube at which $B_x = 0$. An average unit flux tube with $x = -10 R_E$ at the neutral sheet was found to contain only 30 to 40 percent as many particles as an average unit flux tube at $x = -30 R_E$ [Borovsky et al., 1998; Kaufmann et al., 2004b].

[10] A simple numerical example of changes in P_a , T_a , V_f , N_f , $P_a V_f^{5/3}$, and $T_a V_f^{2/3}$ during a reconnection event was presented by *Kaufmann and Paterson* [2006, Figure 9 and Table 1]. In this example, effects of the change in magnetic field topology were separated from the heating that changed the entropy per particle. Both T_a and P_a remained fixed during the topology change. However, the tailward moving plasmoid that was created carried off particles and their associated entropy, so V_f , N_f , and entropy in the resulting Earthward moving closed unit flux tube were smaller than in the original unreconnected closed unit flux tube.

[11] Nonadiabatic particle heating and acceleration in this simple example took place after the topology change. Heating could occur if particles passed through a shock front connected to the small diffusion region in which the topology change took place. There is no change in the entropy per particle during the Earthward collapse in this example because $P_a/n_a^{5/3}$ is constant. However, scattering and fluctuations during the collapse could change $P_a/n_a^{5/3}$ and convert some of the flow energy into thermal energy. The sequence of events ended with a unit flux tube in the inner plasma sheet with a high temperature and a high entropy per particle but with a low entropy per unit flux tube because it contained fewer particles than the original unit flux tube.

1.3. Boltzmann H Function

[12] Some of the questions discussed in the preceding section can be resolved by evaluating Boltzmann's H function

$$H_a(\mathbf{x}, t) = \int f_a(\mathbf{x}, \mathbf{v}, t) \ln[f_a(\mathbf{x}, \mathbf{v}, t)] d^3 v. \quad (5)$$

In the absence of two-particle correlations, Boltzmann's H theorem shows that $H_a(\mathbf{x}, t)$ in an isolated box containing N particles tends to decrease as equilibrium is approached. This is one statement of the second law of thermodynamics. Although two-particle correlations exist, they tend to be small in the very low-density magnetotail. As a result, $H_a(\mathbf{x}, t)$ is expected to fluctuate and to slowly become more negative if $f_a(\mathbf{x}, \mathbf{v}, t)$ evolves toward the equilibrium Maxwell-Boltzmann distribution.

[13] The H function is related to the entropy density or entropy per unit volume by [Huang, 1963]

$$s_a(\mathbf{x}, t) = -k H_a(\mathbf{x}, t). \quad (6)$$

The decrease in $H_a(\mathbf{x}, t)$ as equilibrium is approached therefore corresponds to an increase in $s_a(\mathbf{x}, t)$.

[14] The expression used here for the 10-year averaged entropy in a unit flux tube is $S_{f,a}(\mathbf{x}) = -k H_a(\mathbf{x}) V_f(\mathbf{x})$ and the associated average entropy per particle is $S_{f,a}(\mathbf{x})/N_f(\mathbf{x}) = -k H_a(\mathbf{x})/n_a(\mathbf{x})$. The magnetic field models used to evaluate $V_f(\mathbf{x})$ were determined by averaging the components of \mathbf{B} in the same way that the fluid parameters were averaged. This technique is the same as that used in our previous studies, as illustrated for a 6-year average by *Kaufmann et al.* [2004a, Figure 1]. Our simple \mathbf{B} models are much less sophisticated than those developed by *Tsyganenko* [1990] and *Tsyganenko and Stern* [1996]. However, these simple models have the advantage that they are developed independently for each

data set or subset. Past studies sorted observations according to the bulk flow speed, magnetic flux transport rate, and the IMF direction. Section 4 will show that several features remain unresolved in this paper. Any extension of this work will involve sets of multiple magnetic field and plasma models. The magnetic fields in some members of these sets, such as those based on data taken only during fast flows, differ markedly from the standard empirical models. The use of consistent techniques helps when results from different data sets are compared.

[15] A disadvantage of using these simple \mathbf{B} models is that fluid parameters such as $n_a(\mathbf{x})$, $P_a(\mathbf{x})$, and $H_a(\mathbf{x})$ tend to fluctuate along field lines by 20–30% from their values at the neutral sheet. Fluctuations of these parameters usually are correlated, and are attributed primarily to the need to interpolate between the large $6 \times 6 R_E$ (x, y) boxes used here. The z box thicknesses vary from 0.3 to $1 R_E$. The use of a simple approximation such as $S_{f,a}(\mathbf{x}) = -k H_a(\mathbf{x}) V_f(\mathbf{x})$ rather than an integral of the product of $H_a(\mathbf{x})$ and $ds/\mathbf{B}(\mathbf{x})$, where ds is an incremental distance along \mathbf{B} , reduces the tendency for correlated fluctuations in small regions of a flux tube to become dominant.

[16] The dimensionless parameter that is proportional to the entropy per particle

$$\left(\frac{S}{Nc_v}\right)_{H,a} = \left\langle -\frac{2H_a(\mathbf{x}, t)}{3n_a(\mathbf{x}, t)} \right\rangle \quad (7)$$

also is useful, where $c_v = 3 k/2$ is the average constant volume specific heat per particle for an ideal gas and $\langle \rangle$ indicates a 10-year average. The subscript H is intended to indicate that this parameter was calculated using the measured $H_a(\mathbf{x}, t)$. Equation (7) refers to any volume containing N particles, not only to the volume of a unit flux tube.

[17] The $H_a(\mathbf{x}, t)$ function can be evaluated analytically for a Maxwell-Boltzmann distribution function

$$f_a(\mathbf{x}, \mathbf{v}, t) = n_a(\mathbf{x}, t) \left[\frac{m_a}{2\pi k T_a(\mathbf{x}, t)} \right]^{3/2} \exp \left[-\frac{m_a |\mathbf{v} - \mathbf{V}_a(\mathbf{x}, t)|^2}{2k T_a(\mathbf{x}, t)} \right], \quad (8)$$

where

$$n_a(\mathbf{x}, t) = n_0 \exp \left[\frac{-q_a \phi(\mathbf{x}, t)}{k T_a(\mathbf{x}, t)} \right] \quad (9)$$

is assumed in the magnetotail for particles with charge q_a in the presence of a modest potential \mathbf{E} field. Equations (4), (5), (7), and (8) give

$$\left(\frac{S}{Nc_v}\right)_{P,a} = \ln \left[\frac{2\pi k T_a}{m_a n_a^{2/3}} \right] + 1 = \ln \left[\frac{2\pi P_a}{m_a n_a^{5/3}} \right] + 1, \quad (10)$$

where the subscript P is intended to indicate that this version of the entropy per particle parameter was calculated using the measured $P_a(\mathbf{x}, t)$ and $n_a(\mathbf{x}, t)$, but assuming a Maxwellian rather than the measured non-Maxwellian

$f_a(\mathbf{x}, \mathbf{v}, t)$. Previous entropy studies have generally used this equilibrium $f_a(\mathbf{x}, \mathbf{v}, t)$ assumption.

[18] One reason to evaluate $H_a(\mathbf{x}, t)$ directly from the measured $f_a(\mathbf{x}, \mathbf{v}, t)$ is the lack of reference frame dependence. Uncertainties in evaluating \mathbf{V}_a do not influence the calculation of $H_a(\mathbf{x}, t)$. In addition, although the average $S_{f,a}(\mathbf{x})$ depends upon the use of a magnetic field model, $s_a(\mathbf{x})$, $(S/Nc_v)_{H,a}$ and $(S/Nc_v)_{P,a}$ do not. Some information about the deviation of a plasma from equilibrium also can be obtained by comparing equation (7), which uses the observed non-Maxwellian $f_a(\mathbf{x}, \mathbf{v}, t)$, to equation (10), which is based on the equilibrium $f_a(\mathbf{x}, \mathbf{v}, t)$.

[19] The present study began by calculating 10-year averages of 1-min measurements of $H_i(\mathbf{x}, t)$ and $H_e(\mathbf{x}, t)$, evaluated in SI units, and of many other fluid parameters throughout the $-30 R_E < x < -8 R_E$ region. The Geotail magnetometer [Kokubun *et al.*, 1994] and CPI detectors [Frank *et al.*, 1994] were used. The procedures used and the observations and related uncertainties of the 10-year averages of $H_a(\mathbf{x})$ and $s_a(\mathbf{x})$ are presented in section 2. The 10-year averages $S_{f,a}(\mathbf{x})$, $(S/Nc_v)_{H,i}$, $(S/Nc_v)_{P,i}$ and $(S/Nc_v)_{P,i} - (S/Nc_v)_{H,i}$ are presented in section 3. Each of these parameters reveals information about the physics of the plasma sheet. Finally, the observations are summarized and analyzed in section 4.

2. Data Processing and Uncertainties

2.1. Three-Dimensional Models

[20] Fluid parameters such as n_a , \mathbf{V}_a , P_a , and H_a were evaluated first (equations (1), (2), (3), and (5)). The 1-min data points then were sorted into $6 \times 6 R_E$ x - y boxes. Data in each x - y box were further separated into eight β_x boxes, where β_x is the ordinary plasma β except $B_x^2/2\mu_0$ was used instead of $B^2/2\mu_0$ as the magnetic field pressure. Each fluid parameter was averaged to get its (x, y, β_x) dependence. The x component of the momentum equation was used to calculate the average z distance between the edges of each (x, y, β_x) box and the neutral sheet. The assumptions upon which this procedure is based are that β_x decreases monotonically when moving away from the neutral sheet and that the momentum equation is satisfied when considering long-term averages. The (x, y, β_x) averages then were interpolated onto a preselected (x, y, z) grid to produce a 3-D long-term averaged data based model of all plasma and field parameters in the $-30 < x < -8 R_E$, $-15 < y < 15 R_E$, $0 < |z| < 6 R_E$ region. Northern ($B_x > 0$) and Southern ($B_x < 0$) Hemisphere data points were combined in the runs presented in this paper to increase the number of data points per box. Details of the above procedures were described by Kaufmann *et al.* [2005].

[21] There are advantages and disadvantages associated with our use of long-term averaged data. Averaging is the only way we can create full 3-D data based models of a large region of the plasma sheet using data from one or a few satellites. Long-term averages also smooth out the rapid fluctuations that are present in most plasma sheet variables, revealing average large-scale spatial structures. Such models provide essentially the same information that would be obtained from 10-year averages of each of several hundred plasma and field parameters as seen by an array of 160 satellites that were fixed at our preselected (x, y, z) locations relative to the neutral sheet. Average spatial gradients

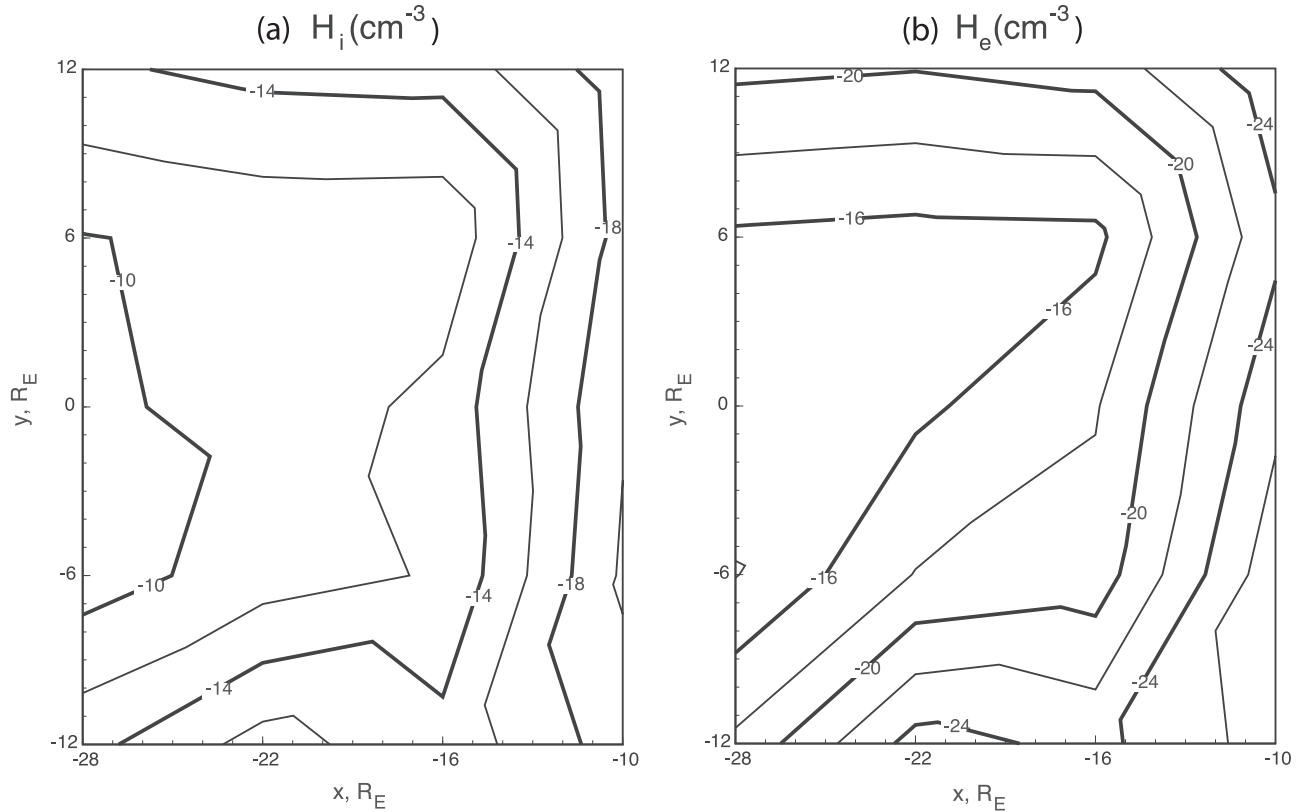


Figure 1. Contour plots of the 10-year averaged Boltzmann H function for (a) ions and (b) electrons near the neutral sheet. This plot is closely related to the entropy density (equation (6)).

therefore can be studied, but no information about time changes can be obtained from the model used in this paper.

[22] Time series data from a single satellite primarily reveals variations of the plasmas that are moving past the satellite location rather than changes that take place when moving with a given plasma element or flux tube. Time series data from an array of several satellites provide the information that is lost when using long-term averages. Such information is needed for event studies and for studies of fluctuations in the plasma and fields. Experimental studies of many important aspects of the physics of the plasma sheet require data from such carefully positioned arrays of satellites.

2.2. $H_a(\mathbf{x})$ and Uncertainties

[23] Figure 1 shows averages over the entire 10-year data set of the newly evaluated fluid parameters $H_i(\mathbf{x})$ and $H_e(\mathbf{x})$. These plots, when multiplied by the constant $-k$ (equation (6)), also show the average spatial dependence of the ion and electron entropy densities. Most plots in this paper are based on particle observations made in the z box closest to the neutral sheet, which was estimated to extend to $|z| = 0.3 R_E$. The fact that the magnitude of $H_e(\mathbf{x})$ is larger than the magnitude of $H_i(\mathbf{x})$ is related to the mass dependence in equation (10). However, it is the change in entropy rather than the absolute magnitude of $H_a(\mathbf{x})$ that is of most interest. The factors $\ln(2\pi/m_a) + 1$ in equation (10) often are treated as arbitrary constants. These constants were retained in equation (10) so that $(S/Nc_v)_{H,a}$ can be compared with $(S/Nc_v)_{P,a}$. Figure 1 shows that spatial changes of the

average ion and of the average electron entropy densities are approximately equal even though the average ion is much more energetic than the average electron.

[24] Since $H_i(\mathbf{x})$ and $H_e(\mathbf{x})$ were averaged independently in each box, comparing box-to-box fluctuations gives a good check on the statistical errors. To examine the reproducibility of the modeling techniques, separate models were made using data from the 5 odd-numbered years and data from the 5 even-numbered years. Comparisons of the box-to-box fluctuations and of differences between the 5-year and 10-year models showed deviations that typically were $\sim 10\%$ and rarely exceeded 20% . The absolute values of typical box-to-box variations of $H_a(\mathbf{x})$ and of variations between the models were therefore $\sim 2 \text{ cm}^{-3}$.

[25] Standard deviations of the individual 1-min data points were comparable to the average values of $H_i(\mathbf{x})$ and $H_e(\mathbf{x})$ in each box. The number of data points per box was used to evaluate standard errors, which were 0.3 cm^{-3} for $H_i(\mathbf{x})$ and 0.4 cm^{-3} for $H_e(\mathbf{x})$. The usefulness of standard error estimates is questionable when dealing with high temporal resolution satellite data because these estimates assume that there is no correlation between consecutive data points. However, *Baumjohann et al.* [1989] showed that fluctuations are so strong in the CPS that the flow velocity exceeds a modest 100 km/s for durations of even one minute less than 10% of the time. The assumption of little correlation between consecutive 1-min averages therefore appears to be reasonable. The fact that the statistical standard errors are substantially smaller than the spatial

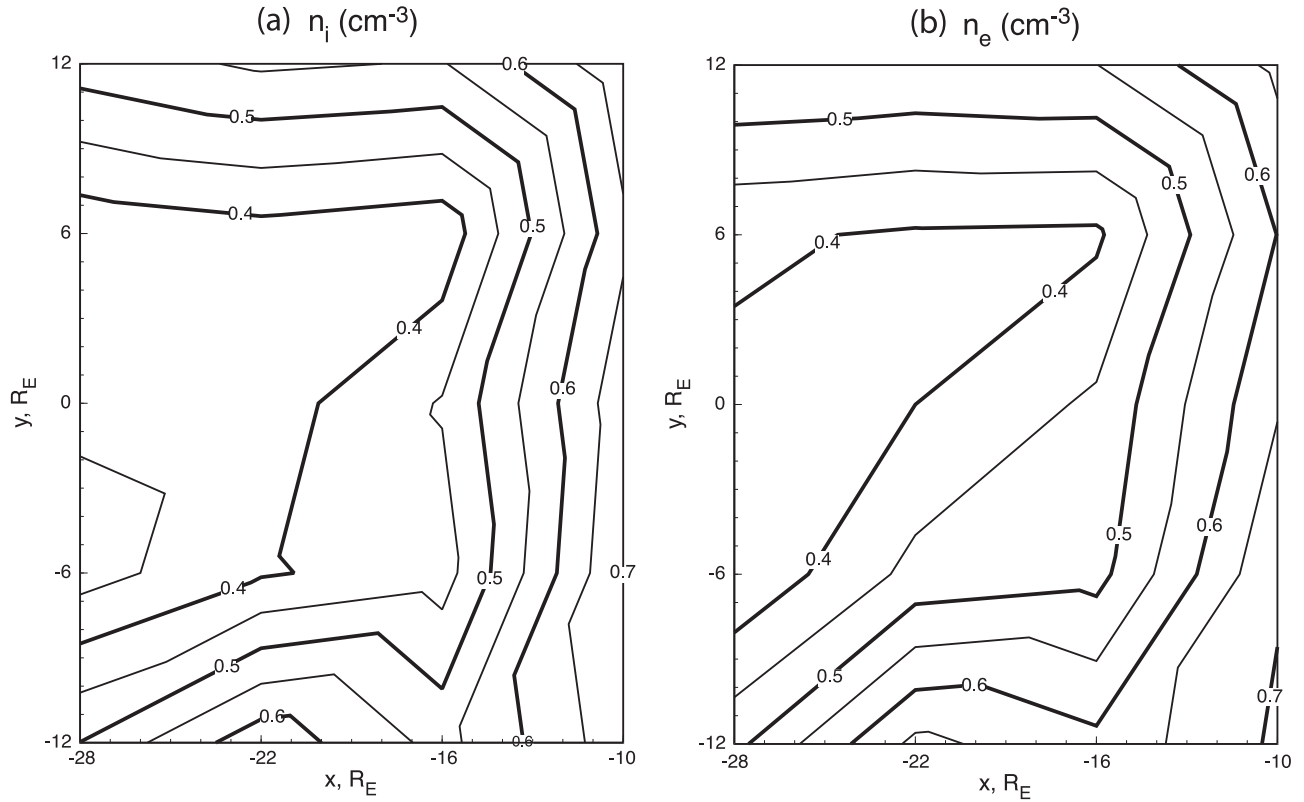


Figure 2. Plots of the average number of (a) ions and (b) electrons per unit volume near the neutral sheet.

variations suggests that the patterns evident in Figure 1 represent real gradients.

[26] Systematic errors can be introduced because the energy range of the satellite detectors is limited. The highest-energy bands were centered at 48 keV with a kinetic energy resolution of $\Delta E_{k,a}/E_{k,a} = 0.1$ [Frank *et al.*, 1994]. The failure to detect >50 keV particles, as seen in the satellite reference frame, can produce artificial asymmetries in $f_a(\mathbf{x}, \mathbf{v}, t)$. This problem was examined in a study of heat fluxes \mathbf{q}_a by evaluating contributions from twelve energy bands [Kaufmann and Paterson, 2008]. Since \mathbf{q}_a is a third-order velocity moment, it is more sensitive to the contributions from high-energy particles than are the variables considered here. It was found that the high-energy limit introduced errors of more than 10% for 10-year averages only in the box centered at $x = -10 R_E$, $y = 0$. This is the box closest to the Earth, where high-energy particles are expected to be most important. Although the high-energy cutoff is not critical in 10-year averages for the region examined here, it is important in studies of events during disturbed periods, when high-energy particle fluxes are much larger than average.

[27] Since the difference between equations (1) and (5) involves only a logarithmic factor, it appears likely that plots of $s_a(\mathbf{x}) = -kH_a(\mathbf{x})$ would be similar to plots of $n_a(\mathbf{x})$. A comparison of Figure 1 and plots of the ion and electron densities (Figure 2) confirms this assumption. Wang *et al.* [2006] presented similar plots of $n_i(\mathbf{x})$. The basic structure of spatial variations in the entropy density therefore can be attributed primarily to similar variations in the particle

density and the simple observation that there is more entropy per unit volume in regions with more particles per unit volume. The dominant features of $s_a(\mathbf{x})$ and $n_a(\mathbf{x})$ near the neutral sheet are that these parameters increase when moving toward the Earth and away from midnight. It will be seen in section 4.3 that the differences between the structures shown in Figures 1 and 2 may be important in identifying regions of particle heating.

3. Other Entropy Parameters

3.1. Entropy Per Unit Flux Tube

[28] Figure 3 shows 10-year averages of the spatial distribution of $S_{f,a}(\mathbf{x}) = -kH_a(\mathbf{x}) V_f(\mathbf{x})$, the entropy per unit flux tube. Since $-kH_a(\mathbf{x})$ increases substantially and $V_f(\mathbf{x})$ increases weakly when moving away from midnight, $S_{f,a}(\mathbf{x})$ also increases toward the flanks. However, $V_f(\mathbf{x})$ decreases more rapidly than $-kH_a(\mathbf{x})$ increases when moving toward the Earth, resulting in the observed Earthward decrease of $S_{f,a}(\mathbf{x})$. The spatial changes in Figure 3 were large compared to the box-to-box fluctuations and to the differences between 5-year and 10-year models, which were typically 0.1–0.2 J/°K.

[29] Since plots of $-kH_a(\mathbf{x})$ and of $n_a(\mathbf{x})$ were seen to be similar (Figures 1 and 2), a plot of $N_f(\mathbf{x}) = n_i(\mathbf{x}) V_f(\mathbf{x})$ naturally also was similar to Figure 3a. Plots of $V_f(\mathbf{x})$ and $N_f(\mathbf{x})$ based on 8 years of Geotail data were included by Kaufmann *et al.* [2004b]. The qualitative relationship between $S_{f,a}(\mathbf{x})$ and $N_f(\mathbf{x})$ shows that the structure of spatial variations in the entropy per unit flux tube can be attributed primarily to similar variations in the particle

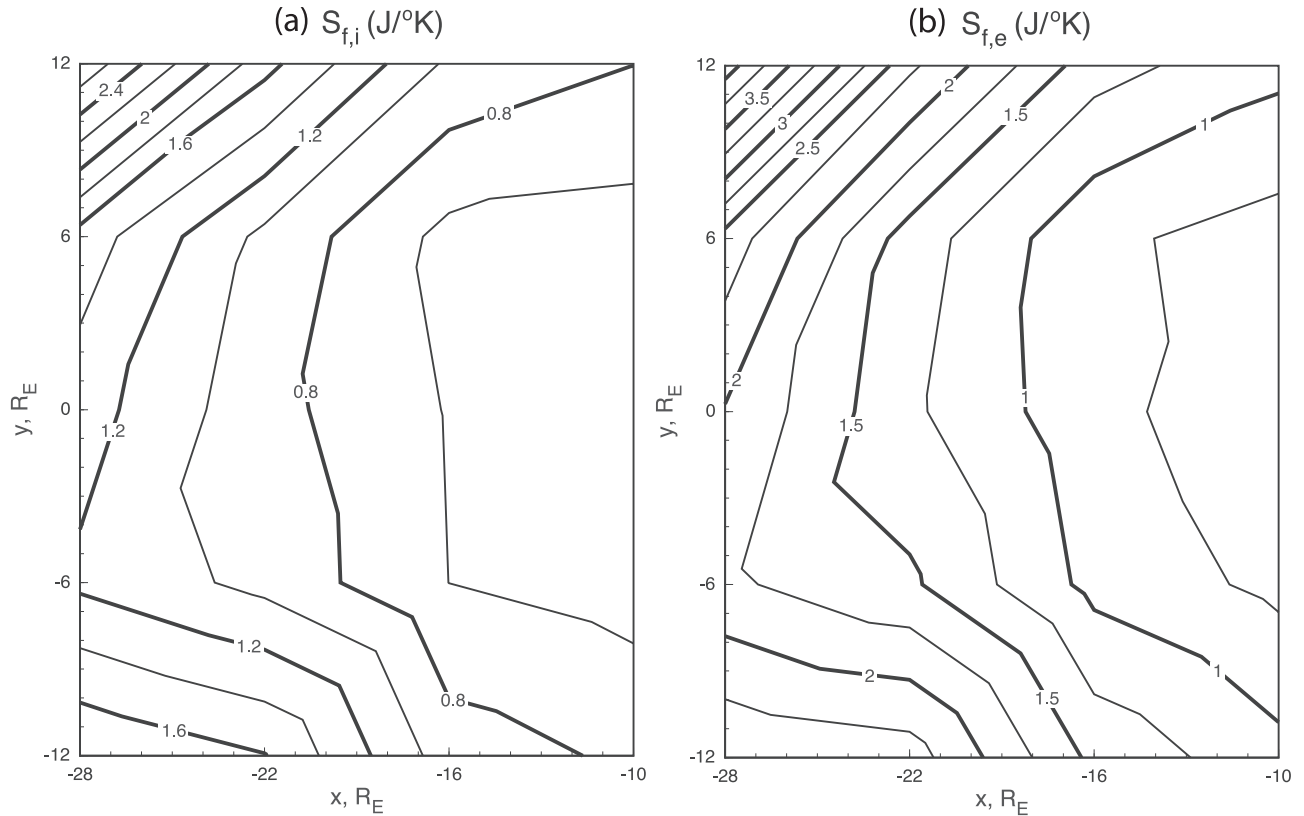


Figure 3. Plots of the average entropy per unit magnetic flux tube for (a) ions and (b) electrons. The magnetic field models used to calculate flux tube volume were based on the same 10-year time averages that were used to calculate the other fluid parameters.

content of unit flux tubes and the observation that there is more entropy within flux tubes that contain more particles. Ion measurements were used to evaluate $N_f(\mathbf{x})$ because they were more reliable than the electron measurements. Since the $V_f(\mathbf{x})$ used to prepare Figure 3 was calculated by combining all 10 years of observations into a single magnetic field model, the fractional standard deviations and standard errors of $S_{f,a}(\mathbf{x})$ are the same as those of $H_a(\mathbf{x})$.

3.2. Entropy Per Particle

[30] Figure 4a shows the long-term average of the dimensionless parameter that is proportional to the average entropy per ion (equation (7)). Neither a \mathbf{B} model nor other information about the region away from the neutral sheet was used to generate Figure 4a, nor was it necessary to determine drift velocities. Figure 4a has smaller gradients than do Figures 1a and 2a because $-kH_i(\mathbf{x})$ and $n_i(\mathbf{x})$ have similar spatial variations. It is the differences between the spatial variations seen in Figures 1a and 2a that produce the gradients in Figure 4a. Only ion data were used when analyzing parameters proportional to the entropy per particle because the fractional changes were much smaller than those of $s_a(\mathbf{x})$ or $S_{f,a}(\mathbf{x})$. Electron data were not sufficiently accurate to reliably determine these gradients.

[31] The average entropy per ion increased when moving Earthward because $-kH_i(\mathbf{x})$ increased more rapidly than did $n_i(\mathbf{x})$. Similarly, the average entropy per ion decreased when moving away from midnight because $n_i(\mathbf{x})$ increased more rapidly than did $-kH_i(\mathbf{x})$ in this direction. Plots based on the

two separate 5-year averaged models showed similar trends. Box-to-box fluctuations and comparisons of the 5-year and 10-year models showed typical variations in $(S/Nc_v)_{H,i}$ of 0.1–0.2. The standard deviation of individual 1-min data points was 0.9, and the standard error was 0.02. As in the previous plots, the fact that the observed variations were significantly larger than the standard error suggests that the gradients are real rather than just statistical errors due to sampling from a Gaussian distribution.

[32] Dealing with the average entropy per ion removes the effects of the simple observation that there is more entropy per unit volume or per unit flux tube when there are more particles per unit volume or per unit flux tube. The spatial gradient of the entropy per ion suggests that ions are being heated within the plasma sheet as they move Earthward. However, there are other possible interpretations of Figure 4a, as will be discussed in section 4.3.

3.3. Deviations From Equilibrium

[33] The observed non-Maxwellian $f_i(\mathbf{x}, \mathbf{v}, t)$ was used to evaluate $(S/Nc_v)_{H,i}$. In contrast, $(S/Nc_v)_{P,i}$ is the dimensionless average entropy per ion that would exist in a plasma with the observed $P_i(\mathbf{x}, t)$ and $n_i(\mathbf{x}, t)$ if $f_i(\mathbf{x}, \mathbf{v}, t)$ was a Maxwellian (Figure 4b). Typical nonequilibrium features seen in $f_i(\mathbf{x}, \mathbf{v}, t)$ include asymmetric stretching of constant f_i contours in one direction, bulk flows, plateaus or other remnants of stabilized or partially mirrored ion beams, and enhanced high-energy tails that often are represented by a

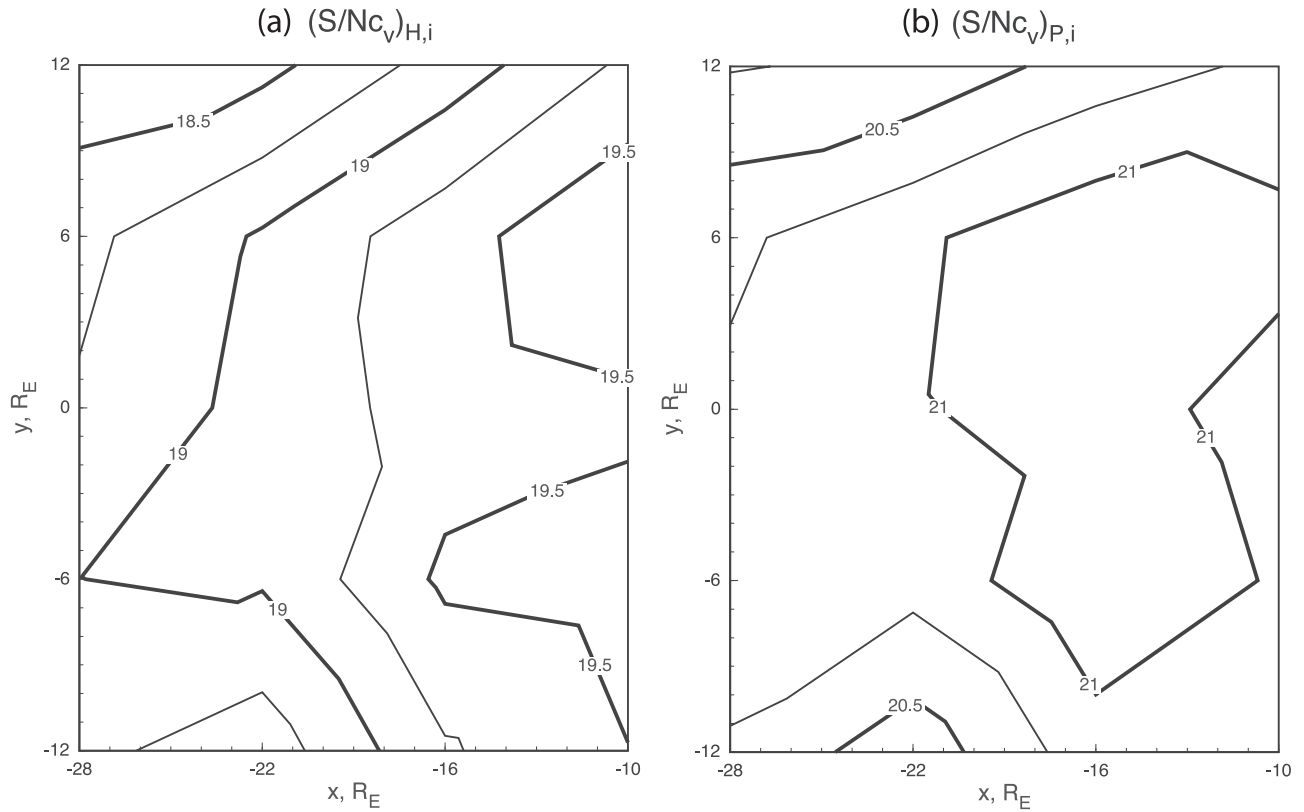


Figure 4. (a) The average dimensionless entropy per ion parameter near the neutral sheet, as determined using the Boltzmann H function and equation (7). (b) The average dimensionless entropy per ion parameter that would be present in a plasma with a Maxwell-Boltzmann distribution function and the measured pressure and density, as determined by equation (10).

kappa distribution [Nakamura *et al.*, 1991; Mukai *et al.*, 1998; Nagai *et al.*, 1998].

[34] As was noted in section 1.3, Boltzmann's H theorem or the second law of thermodynamics shows that the entropy density or $-kH$ of gas in an isolated box would tend to increase toward a maximum as the system evolves toward equilibrium. As a result, $(S/Nc_v)_{H,i}$ would approach $(S/Nc_v)_{P,i}$ as the gas evolves toward a Maxwell-Boltzmann distribution (equation (8)). Differences between $(S/Nc_v)_{P,i}$ and $(S/Nc_v)_{H,i}$ for each 1-min data point were averaged to generate Figure 5. This dimensionless parameter is a measure of the deviation of the observed entropy per ion from the maximum entropy that would be attained at equilibrium in a plasma with the same $n_i(\mathbf{x})$ and $P_i(\mathbf{x})$. Figure 5 shows that $\delta(S/Nc_v)_i = (S/Nc_v)_{P,i} - (S/Nc_v)_{H,i}$ near the neutral sheet decreased from 2.0 at $x = -28 R_E$ to 1.4 at $x = -10 R_E$. Plots from the two 5-year averaged runs were very similar to the 10-year average in Figure 5. Possible interpretations of this decrease will be discussed in section 4.5.

4. Summary and Analysis

4.1. H_a and the Entropy Density

[35] The Boltzmann H function is the new parameter upon which this paper is based. One advantage of using $H_a(\mathbf{x}, t)$ to study entropy is that its evaluation involves a single integration that is based only on the measured distribution function $f_a(\mathbf{x}, \mathbf{v}, t)$. There is no need to evaluate

$V_a(\mathbf{x}, t)$ or $P_a(\mathbf{x}, t)$ to obtain $s_a(\mathbf{x}, t)$. Figure 1 showed the spatial dependence of the 10-year averaged ion and electron $H_a(\mathbf{x})$ as seen at the neutral sheet. Since $s_a(\mathbf{x}) = -kH_a(\mathbf{x})$ is the average entropy per unit volume and k is Boltzmann's constant, Figure 1 also illustrated the long-term averaged spatial variation of $s_a(\mathbf{x})$.

[36] A comparison of $s_a(\mathbf{x})$ with Figure 2, the spatial dependence of the particle densities $n_a(\mathbf{x})$, showed that gradients in $s_a(\mathbf{x})$ were primarily reflections of similar gradients in $n_a(\mathbf{x})$. For comparison to other parameters it is noted that $-kH_a(\mathbf{x})$ or $s_a(\mathbf{x})$ increased by almost a factor of two between $x = -28 R_E$ and $x = -10 R_E$ and also increase by $\sim 50\%$ between midnight and the flanks beyond $x = -15$ to $-20 R_E$. Physically it is the magnitude of the change in entropy that is the important parameter. It therefore is interesting to note that the spatial changes of entropy per unit volume were comparable for ions and electrons even though $T_i(\mathbf{x})$ averaged ~ 7 times $T_e(\mathbf{x})$ [Baumjohann *et al.*, 1989; Kaufmann *et al.*, 2005].

4.2. Entropy Per Unit Flux Tube

[37] Figure 3 shows the spatial dependence of the entropies of ions and electrons contained in a tube containing 1 Wb of magnetic flux, $S_{f,a}(\mathbf{x}) = -kH_a(\mathbf{x}) V_f(\mathbf{x})$. In this expression, $V_f(\mathbf{x})$ is the volume of a unit flux tube that crosses the neutral sheet at \mathbf{x} . Since the relationship between $S_{f,a}(\mathbf{x})$ and $N_f(\mathbf{x})$ is the same as the relationship between $s_a(\mathbf{x})$ and $n_a(\mathbf{x})$, the spatial structure of $S_{f,a}(\mathbf{x})$ also was

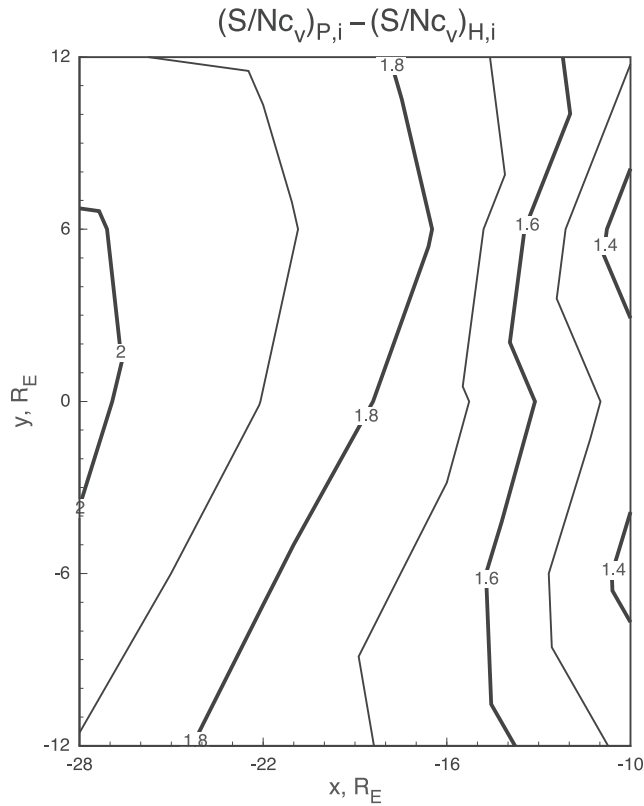


Figure 5. The difference $(S/Nc_v)_{P,i} - (S/Nc_v)_{H,i}$ for each 1-min data point was averaged for the 10-year data set. This difference is a measure of the deviation of the plasma from equilibrium.

primarily a reflection of the similar spatial structure of $N_f(\mathbf{x})$. At midnight between $x = -28 R_E$ and $x = -10 R_E$ $S_{f,a}(\mathbf{x})$ decreased by a factor of more than 2, $s_a(\mathbf{x})$ increased by a factor of 2, and $V_f(\mathbf{x})$ decreased by a factor of 6 [Kaufmann et al., 2004b, Figure 1]. It was this decrease near midnight in the long-term averaged entropy per unit flux tube that led Erickson and Wolf [1980] to the concept of a pressure balance inconsistency. Between midnight and the flanks $S_{f,a}(\mathbf{x})$ increased, as did $-kH_a(\mathbf{x})$ because $V_f(\mathbf{x})$ had only a weak y dependence.

[38] Although the observed Earthward decreases in $S_{f,a}(\mathbf{x})$ and $N_f(\mathbf{x})$ have been known for years, the cause of this structure is not fully resolved. Studies of the plasma sheet often assumed that there were two or more sources with substantially different properties. Particles with different energies from multiple sources follow different drift paths to produce the $f_a(\mathbf{x}, \mathbf{v}, t)$ seen at a given observation point. Sources that have been considered include the LLBL and the distant tail or one of several related pairs of sources in the distant tail. These distant tail sources can consist of low-density bubbles and high-density blobs, reconnected and unreconnected flux tubes, or regions of fast and of slow plasma transport.

[39] Spence and Kivelson [1993], Garner et al. [2003], and Wang et al. [2006] considered the mixing of particles from a relatively uniform LLBL source and a relatively uniform distant tail source. These studies emphasized the importance of the energy dependence of cross tail drifts.

Such drifts cause particles to enter and leave each moving flux tube, producing gradients in $S_{f,a}(\mathbf{x})$ and $N_f(\mathbf{x})$.

[40] Reconnection is a process that generates multiple distant tail sources and provides a natural way to explain why N_f is so much smaller at $x = -10 R_E$ than at $x = -30 R_E$. A plasmoid carries off both particles and their associated entropy when a unit flux tube reconnects. The resulting closed reconnected unit flux tube therefore contains fewer particles and usually less total entropy than nearby closed unit flux tubes that did not reconnect. In addition, the newly reconnected flux tube is moving Earthward when it leaves the reconnection region. It has been suggested that these reconnected flux tubes or bubbles with small N_f and $PV_f^{5/3}$ reach the lowest altitudes before their Earthward motion ends [Pontius and Wolf, 1990; Chen and Wolf, 1993; Sergeev et al., 1996; Shiokawa et al., 1997]. As a result, the lowest-altitude region becomes populated primarily by these low N_f and low $PV_f^{5/3}$ flux tubes. This mechanism therefore emphasizes the $PV_f^{5/3}$ -dependent differences in drift velocities of flux tubes from patchy tail sources rather than the flow of particles into or out of flux tubes from relatively uniform tail and LLBL sources to explain the observed gradients in N_f and $PV_f^{5/3}$.

4.3. Entropy Per Particle Derived From H

[41] Figure 4a shows that the dimensionless ratio $(S/Nc_v)_{H,i}$, that is proportional to the average entropy per ion, increased from $x = -28 R_E$ to $x = -10 R_E$ and decreased between midnight and the flanks. The changes in $(S/Nc_v)_{H,i}$ were smaller than the changes in $s_i(\mathbf{x})$ and $n_i(\mathbf{x})$ because $(S/Nc_v)_{H,i}$ is proportional to the ratio of these two parameters that exhibited similar spatial dependencies (equation (7)).

[42] The requirement to explain the gradients seen in Figure 4a places a constraint on multiple source mixing mechanisms. Most studies have assumed that the average entropy per ion was conserved along particle or flux tube drift paths. Since we concluded that gradients in $s_a(\mathbf{x})$ and in $S_{f,a}(\mathbf{x})$ were primarily associated with changes in $n_a(\mathbf{x})$ and in $N_f(\mathbf{x})$, respectively, any mechanism that explained the structure of these two density parameters would also explain the basic structure of the related entropy parameters. However, changes in the entropy per ion are not influenced by changes in particle densities.

[43] Many mechanisms already have been suggested that change the average entropy of particles while they pass through the region studied here. The well-known outflow of cold ionospheric ions will change the average entropy per ion within a flux tube. The absorption of wave energy will heat plasma in a flux tube. The mechanism proposed by Goertz and Smith [1989] suggested that the absorption of waves generated at the PSBL is an important CPS heating process. The braking of flow at low altitudes combined with fluctuations comparable to an ion gyroradius could convert some of the bulk flow energy into thermal energy. A number of papers [e.g., Lysak and Song, 2005] discussed the transport of energy from the plasma sheet to the ionosphere by Alfvén waves. This process will cool plasma sheet flux tubes. Cross-tail diffusion that mixes low-energy ions from LLBL sources and high-energy ions from magnetotail sources will vary the average entropy along drift paths. This diffusion can be caused by fluctuations in $V_y(\mathbf{x}, t)$, the cross-tail component of the bulk flow velocity. The presence

of thick regions dominated by LLBL particles at both the dawn and dusk flanks during northward IMF suggests that cross-tail diffusion is important [Wang *et al.*, 2006].

[44] The spatial structure in Figure 4a fits particularly well with the suggestion that plasma is heated during substorms [Huang *et al.*, 1992]. Most substorms take place near midnight, which is where $(S/Nc_v)_{H,i}$ exhibits a maximum. Heating that takes place during substorm injections would continue as plasma moves toward the Earth. The substorm heating process therefore also would naturally explain the observed Earthward increase in the average entropy per ion.

4.4. Entropy Per Particle Derived From P and n

[45] Figure 4b shows the entropy per ion obtained by evaluating $P_i(\mathbf{x}, t)$ and $n_i(\mathbf{x}, t)$, using equation (10), and then averaging the results. This expression gives the entropy that would exist in a Maxwellian plasma with the observed density and pressure, and is usually used to evaluate entropy. Boltzmann's H theorem and the second law of thermodynamics showed that $(S/Nc_v)_{P,i}$ can be considered as the maximum average entropy per ion that can be attained in a plasma with the measured $P_i(\mathbf{x})$ and $n_i(\mathbf{x})$. Figure 4 shows that $(S/Nc_v)_{P,i}$ was larger than $(S/Nc_v)_{H,i}$ and that both decreased near the flanks and increased when moving Earthward. There are, however, significant differences between the variations of $(S/Nc_v)_{H,i}$ and $(S/Nc_v)_{P,i}$ that will be discussed in the next section. The magnitudes of changes in the dimensionless entropy per ion parameters shown in Figure 4 may appear to be small. However, since $(S/Nc_v)_{P,i}$ is determined by $\ln(P_i/n_i^{5/3})$, a change of $(S/Nc_v)_{P,i}$ by 0.5 corresponds to a change of $(P_i/n_i^{5/3})$ by a factor $\exp(0.5) = 1.6$.

[46] Equation (10) also shows why changes in the electron and ion entropy per particle are so similar even though ions are much more energetic than electrons and changes in the entropy parameters $P_a/n_a^{5/3}$ and $P_aV_f^{5/3}$ are much larger for ions than for electrons. Equation (10) shows that the change in entropy is $\ln(T_{a2}n_1^{2/3}/T_{a1}n_2^{2/3})$ between an initial state with density $n_i = n_e = n_1$ and temperatures T_{i1} , T_{e1} and a final state with density $n_i = n_e = n_2$ and temperatures T_{i2} , T_{e2} . The changes in electron and ion entropies therefore are equal as long as the ratio T_i/T_e remains fixed, leading to $T_{i2}/T_{i1} = T_{e2}/T_{e1}$. It was previously shown [Baumjohann *et al.*, 1989] that T_i/T_e remains ~ 7 in the CPS. Kaufmann *et al.* [2005] noted that there was a tendency for T_i/T_e to decrease slightly when moving Earthward near the neutral sheet. This relative increase in T_e implies that the electron entropy increases slightly faster than the ion entropy when moving Earthward.

[47] The fact that ion and electron entropy changes are equal provided that T_i/T_e remains constant also can be seen by assuming that the entropy change is reversible rather than that the plasma is Maxwellian. For a reversible change $dS_a = dQ_a/T_a$ where dS_a and dQ_a refer to the change of entropy and the heat absorbed by a fixed group of N ions or N electrons that remain within a box. If $T_i/T_e = 7$ throughout the process then $dS_i/dS_e = dQ_i/7dQ_e$ so the ion and electron entropy changes will be equal provided that ions absorb 7 times as much heat as do electrons. The first law of thermodynamics gives $dQ_a = C_v dT_a + P_a dV_a$, where C_v is the constant volume heat capacity of the N particles. The

ideal gas equation (4) and the requirements that $N_i = N_e$ and $V_i = V_e$ give $P_i/P_e = T_i/T_e$ and $dQ_i/dQ_e = 7$, so that $dS_i = dS_e$.

[48] Most previous entropy studies have neglected electrons because T_e , $P_e/n_e^{5/3}$, and $P_eV_f^{5/3}$ are much smaller than T_i , $P_i/n_i^{5/3}$, and $P_iV_f^{5/3}$. The finding that electrons and ions contribute nearly equally to changes in $s_a(\mathbf{x})$ and $S_{f,a}(\mathbf{x})$ does not, however, alter most previous conclusions. Since dQ_i is much larger than dQ_e , the heat sources or sinks needed to explain the observed entropy changes are almost all associated with ion heating. Unless a study is specifically directed toward electron thermodynamics, it probably is sufficient to simply assume that the total entropy change is twice the ion entropy change.

4.5. Deviation From Equilibrium

[49] Figure 5 shows a smooth Earthward decrease but little y dependence of $\delta(S/Nc_v)_i = (S/Nc_v)_{P,i} - (S/Nc_v)_{H,i}$, a measure of the deviation of the observed plasma from equilibrium. The Earthward decrease in $\delta(S/Nc_v)_i$ near the neutral sheet shows that the average plasma at $x = -10 R_E$ is closer to equilibrium than the average plasma at $x = -28 R_E$. The substantial difference between $(S/Nc_v)_{H,i}$ and $(S/Nc_v)_{P,i}$ also shows that the commonly used Maxwellian assumption (equation (10)) or use of the parameter $P_i/n_i^{5/3}$ significantly overestimates the entropy per ion, and that this overestimate is larger at $x = -28 R_E$ than at $x = -10 R_E$. The structure seen in Figure 5 suggests, but does not prove, that each group of ions was slowly approaching equilibrium as it moved Earthward.

[50] Ion scattering can be produced through interactions with plasma waves, with small-scale spatial structures, or through chaotic interactions near the neutral sheet, where ion gyroradii can approach the radius of curvature of a magnetic field line. Our previous studies [e.g., Kaufmann *et al.*, 2003, 2005] concluded that both ions and electrons undergo substantial scattering throughout the plasma sheet. Conservation of the energy invariant $\lambda_a = E_{k,a}V_f^{2/3}$ assumes that elastic scattering maintains a nearly isotropic $f_a(\mathbf{x}, \mathbf{v}, t)$, where $E_{k,a}(\mathbf{x})$ is the average kinetic energy per particle of species a [Wolf, 1983]. Particle scattering tends to make an initially anisotropic $f_a(\mathbf{x}, \mathbf{v}, t)$ more nearly isotropic, and therefore tends to bring the plasma closer to equilibrium. Scattering events also can cause the energy dependence of an isotropic non-Maxwellian $f_a(\mathbf{x}, \mathbf{v}, t)$ to become more nearly Maxwellian.

[51] A deviation from equilibrium is not the only possible reason why the measured $\delta(S/Nc_v)_a$ could be nonzero. Several instrument calibration and data processing effects were considered. Particle detector calibration errors change $f_a(\mathbf{x}, \mathbf{v}, t)$, $n_a(\mathbf{x}, t)$, $H_a(\mathbf{x}, t)$ and $P_a(\mathbf{x}, t)$. However, multiplication of $f_a(\mathbf{x}, \mathbf{v}, t)$ by a correction factor r would add a factor $-(2/3) \ln r$ to both equations (7) and (10), so would contribute nothing to the differences plotted in Figure 5. Errors in determining $T_a(\mathbf{x}, t)$ would change equations (7) and (10) differently, but the effect is only logarithmic. It therefore appears that an unreasonable temperature correction would be needed to change $\delta(S/Nc_v)_i$ enough to shift the contours in Figure 5 to zero.

[52] The use of different data averaging techniques also was considered. Figure 4 was prepared by averaging the 1-min observations of $(S/Nc_v)_{H,i}$ and $(S/Nc_v)_{P,i}$. Equations (1), (4), and (5) show that there are correlations between $n_a(\mathbf{x}, t)$

and both $H_a(\mathbf{x}, t)$ and $P_a(\mathbf{x}, t)$, so different averaging techniques may produce significant differences in plots of $\delta(S/Nc_v)_a$. To test the sensitivity of the results in Figure 5 to modifications of the averaging techniques we tried using $\langle H_a \rangle / \langle n_a \rangle$ instead of $\langle H_a / n_a \rangle$ when calculating averages in equation (7) (Figure 4a) and $\langle P_a \rangle / \langle n_a \rangle^{5/3}$ instead of $\langle P_a / n_a^{5/3} \rangle$ in equation (10) (Figure 4b). These changes produced a plot of $\delta(S/Nc_v)_i$ with similar trends, but with absolute values ~ 0.2 larger than is shown in Figure 5. The general conclusions concerning entropy per ion therefore do not depend strongly on this aspect of the averaging technique.

[53] A plot similar to Figure 5 also was prepared for electrons. The uncertainties were comparable to the magnitudes of $\delta(S/Nc_v)_e$ so the plot was not considered to be reliable. One consistent finding was that the magnitude of $\delta(S/Nc_v)_e$ was smaller than the magnitude of $\delta(S/Nc_v)_i$. This suggests that the average $f_e(\mathbf{x}, \mathbf{v}, t)$ was closer to a Maxwell-Boltzmann equilibrium than was the average $f_i(\mathbf{x}, \mathbf{v}, t)$.

4.6. Principal Conclusions

[54] The use of 10-year averages restricted us to spatial rather than temporal studies of the plasma sheet. Previous long-term averaged studies revealed much of what is now known about the basic structure of plasmas, fields, electric currents, energy densities, and transport in the plasma sheet.

[55] Average spatial variations of four entropy parameters were examined between $x = -28 R_E$ and $x = -10 R_E$. Each of the four parameters has a different physical significance and showed a different spatial structure. Gradients in $s_a(\mathbf{x})$, the ion and electron entropies per unit volume, were associated primarily with similar gradients in the particle densities $n_a(\mathbf{x})$. Similarly, gradients in $S_{f,a}(\mathbf{x})$, the ion and electron entropies per unit flux tube, were associated with gradients in $N_f(\mathbf{x})$, the particle content of unit flux tubes. Both $s_a(\mathbf{x})$ and $n_a(\mathbf{x})$ increased when moving Earthward while $V_f(\mathbf{x})$, the volume of a unit flux tube, decreased more rapidly than $s_a(\mathbf{x})$ and $n_a(\mathbf{x})$ increased. These gradients resulted in Earthward decreases in $S_{f,a}(\mathbf{x})$ and $N_f(\mathbf{x})$. It often has been assumed that such gradients can be explained by adiabatic processes. Studies based on the mixing of a relatively uniform LLBL source and of a relatively uniform tail source emphasized adiabatic energy-dependent particle drifts. Studies of patchy tail sources such as bubbles and blobs, reconnected and unreconnected flux tubes, or fast and slow transport regions emphasized the conservation of $PV_f^{5/3}$ in unit flux tubes.

[56] Gradients of $(S/Nc_v)_{H,i}$, which are proportional to the average entropy per ion, were weaker than gradients of the average entropy per unit volume or per unit flux tube. The process that most naturally appears capable of explaining the spatial structure of $(S/Nc_v)_{H,i}$ near the neutral sheet involves nonadiabatic plasma heating during substorms.

[57] Gradients of $\delta(S/Nc_v)_i = (S/Nc_v)_{P,i} - (S/Nc_v)_{H,i}$, a measure of the deviation of the plasma from equilibrium, also were found. The $(S/Nc_v)_{P,i}$ parameter is proportional to the average entropy per ion in a Maxwellian plasma with the observed pressure and density. $(S/Nc_v)_{H,i}$ and $(S/Nc_v)_{P,i}$ exhibited qualitatively similar spatial variations, but the magnitudes of their gradients were different. The variations of $\delta(S/Nc_v)_i$ suggested that distribution functions evolved substantially toward equilibrium as ions moved through the

region studied. The magnitude and gradient of $\delta(S/Nc_v)_i$ also showed that the Maxwellian assumption significantly overestimates the entropy per ion and that this overestimate is larger at $x = -28 R_E$ than at $x = -10 R_E$. The evolution of $\delta(S/Nc_v)_i$ can be produced by interactions with waves, fluctuations, or chaotic orbit scattering. Elastic scattering reduces any anisotropies in an initial $f_a(\mathbf{x}, \mathbf{v}, t)$. Previous observations showed that long-term averages of $f_a(\mathbf{x}, \mathbf{v}, t)$ were nearly isotropic at the neutral sheet even though a significant portion of the 1-min averaged $f_a(\mathbf{x}, \mathbf{v}, t)$ data points in the CPS exhibited anisotropic features. Scattering processes also can cause the energy dependence of an initially non-Maxwellian $f_a(\mathbf{x}, \mathbf{v}, t)$ to become more nearly Maxwellian.

[58] One other finding was that although plasma sheet ions dominate gradients of the energy density, gradients of the entropy densities of electrons and ions are approximately equal. This feature was attributed to the observation that T_i/T_e was nearly constant in the region studied.

[59] It may be possible to clarify some of the remaining unresolved questions by creating subsets of the observations corresponding to different geophysical conditions, but the present paper only examined averages of all 10 years of available data. Since the H function proved to be a useful parameter that is just as easy to evaluate as other fluid parameters, it seems worthwhile to include $H_a(\mathbf{x}, t)$ in the set of parameters that are routinely evaluated when processing satellite particle data.

[60] **Acknowledgments.** This material is based upon work at the University of New Hampshire that was supported by the National Science Foundation under grant ATM-0741791. Research at the University of Iowa and at Hampton University was supported by the National Aeronautics and Space Administration under grant NAG5-11485. The authors would like to thank L. A. Frank, who developed the Geotail Comprehensive Plasma Instrumentation and was instrumental in initiating this series of studies, and T. Nagai, who supplied the suitably averaged Geotail magnetic field measurements. We also would like to thank the reviewers for making constructive suggestions that were incorporated into this paper.

[61] Wolfgang Baumjohann thanks the reviewers for their assistance in evaluating this paper.

References

- Baumjohann, W., G. Paschmann, and C. A. Cattell (1989), Average plasma properties in the central plasma sheet, *J. Geophys. Res.*, *94*, 6597–6606.
- Borovsky, J. E., M. F. Thomsen, R. C. Elphic, T. E. Cayton, and D. J. McComas (1998), The transport of plasma sheet material from the distant tail to geosynchronous orbit, *J. Geophys. Res.*, *103*, 20,297–20,331.
- Chen, C. X., and R. A. Wolf (1993), Interpretation of high-speed flows in the plasma sheet, *J. Geophys. Res.*, *98*, 21,409–21,419.
- Erickson, G. M., and R. A. Wolf (1980), Is steady convection possible in the Earth's magnetotail?, *Geophys. Res. Lett.*, *7*, 897–900.
- Frank, L. A., K. L. Ackerson, W. R. Paterson, J. A. Lee, M. R. English, and G. L. Pickett (1994), The comprehensive plasma instrumentation (CPI) for the GEOTAIL spacecraft, *J. Geomag. Geoelectr.*, *46*, 23–37.
- Garner, T. W., R. A. Wolf, R. W. Spiro, M. F. Thomsen, and H. Korth (2003), Pressure balance inconsistency exhibited in a statistical model of magnetospheric plasma, *J. Geophys. Res.*, *108*(A8), 1331, doi:10.1029/2003JA009877.
- Goertz, C. K., and W. Baumjohann (1991), On the thermodynamics of the plasma sheet, *J. Geophys. Res.*, *96*, 20,991–20,998.
- Goertz, C. K., and R. A. Smith (1989), The thermal catastrophe model of substorms, *J. Geophys. Res.*, *94*, 6581–6596.
- Huang, C. Y., L. A. Frank, G. Rostoker, J. Fennell, and D. G. Mitchell (1992), Nonadiabatic heating of the central plasma sheet at substorm onset, *J. Geophys. Res.*, *97*, 1481–1495.
- Huang, K. (1963), *Statistical Mechanics*, John Wiley, New York.
- Kaufmann, R. L., and W. R. Paterson (2006), Magnetic flux and particle transport in the plasma sheet, *J. Geophys. Res.*, *111*, A10214, doi:10.1029/2006JA011734.

- Kaufmann, R. L., and W. R. Paterson (2008), Ion heat flux and energy transport near the magnetotail neutral sheet, *J. Geophys. Res.*, *113*, A05207, doi:10.1029/2007JA012929.
- Kaufmann, R. L., W. R. Paterson, and L. A. Frank (2003), Birkeland currents in the plasma sheet, *J. Geophys. Res.*, *108*(A7), 1299, doi:10.1029/2002JA009665.
- Kaufmann, R. L., W. R. Paterson, and L. A. Frank (2004a), Magnetization of the plasma sheet, *J. Geophys. Res.*, *109*, A09212, doi:10.1029/2003JA010148.
- Kaufmann, R. L., W. R. Paterson, and L. A. Frank (2004b), Pressure, volume, density relationships in the plasma sheet, *J. Geophys. Res.*, *109*, A08204, doi:10.1029/2003JA010317.
- Kaufmann, R. L., W. R. Paterson, and L. A. Frank (2005), Relationships between the ion flow speed, magnetic flux transport rate, and other plasma sheet parameters, *J. Geophys. Res.*, *110*, A09216, doi:10.1029/2005JA011068.
- Kokubun, S., T. Yamamoto, M. H. Acuna, K. Hayashi, K. Shiokawa, and H. Kawano (1994), The Geotail magnetic field experiment, *J. Geomag. Geoelectr.*, *46*, 7–21.
- Lysak, R. L., and Y. Song (2005), Nonlocal interactions between electrons and Alfvén waves on auroral field lines, *J. Geophys. Res.*, *110*, A10S06, doi:10.1029/2004JA010803.
- Mukai, T., T. Yamamoto, and S. Machida (1998), Dynamics and kinetic properties of plasmoids and flux ropes: GEOTAIL observations, in *New Perspectives on the Earth's Magnetotail*, *Geophys. Monogr. Ser.*, vol. 105, edited by A. Nishida, D. N. Baker, and S. W. H. Cowley, pp. 117–137, AGU, Washington, D. C.
- Nagai, T., M. Fujimoto, Y. Saito, S. Machida, T. Terasawa, R. Nakamura, T. Yamamoto, T. Mukai, A. Nishida, and S. Kokubun (1998), Structure and dynamics of magnetic reconnection for substorm onsets with Geotail observations, *J. Geophys. Res.*, *101*, 4419–4440.
- Nakamura, M., G. Paschmann, W. Baumjohann, and N. Sckopke (1991), Ion distributions and flows near the neutral sheet, *J. Geophys. Res.*, *96*, 5631–5649.
- Pontius, D. H., and R. A. Wolf (1990), Transient flux tubes in the terrestrial magnetosphere, *Geophys. Res. Lett.*, *17*, 49–52.
- Rossi, B., and S. Olbert (1970), *Introduction to the Physics of Space*, McGraw-Hill, New York.
- Sergeev, V. A., V. Angelopoulos, J. T. Gosling, C. A. Cattell, and C. T. Russell (1996), Detection of localized, plasma-depleted flux tubes or bubbles in the midtail plasma sheet, *J. Geophys. Res.*, *101*, 10,817–10,826.
- Shiokawa, K., W. Baumjohann, and G. Haerendel (1997), Braking of high-speed flows in the near-Earth tail, *Geophys. Res. Lett.*, *24*, 1179–1182.
- Spence, H. E., and M. G. Kivelson (1993), Contributions of the low-latitude boundary layer to the finite width magnetotail convection model, *J. Geophys. Res.*, *98*, 15,487–15,496.
- Tsyganenko, N. A. (1990), Quantitative models of the magnetospheric magnetic field: Methods and results, *Space Sci. Rev.*, *54*, 75–186.
- Tsyganenko, N. A., and D. P. Stern (1996), Modeling the global magnetic field of the large-scale Birkeland current systems, *J. Geophys. Res.*, *101*(A12), 27,187–27,198.
- Wang, C.-P., L. R. Lyons, J. M. Weygand, T. Nagai, and R. W. McEntire (2006), Equatorial distributions of the plasma sheet ions, their electric and magnetic drifts, and magnetic fields under different interplanetary magnetic field Bz conditions, *J. Geophys. Res.*, *111*, A04215, doi:10.1029/2005JA011545.
- Wolf, R. A. (1983), The quasi-static (slow-flow) region of the magnetosphere, in *Solar-Terrestrial Physics*, edited by R. L. Carovillano and J. M. Forbes, pp. 303–368, D. Reidel, Hingham, Mass.

R. L. Kaufmann, Department of Physics, University of New Hampshire, Durham, NH 03824, USA. (dick.kaufmann@unh.edu)

W. R. Paterson, Department of Atmospheric and Planetary Sciences, Hampton University, Hampton, VA 23668, USA.